Electron mobility measurement in *n*-GaAs at low-temperature impurity breakdown

V. Novák and M. Cukr
Institute of Physics AS CR, Cukrovarnická 10, 162 00 Praha 6, Czech Republic

D. Schowalter and W. Prettl
Institut für Experimentelle und Angewandte Physik, Universität Regensburg, 93040 Regensburg, Germany

(Received 26 July 2000)

Using a combination of the standard Hall technique and the photoluminescence imaging of galvanomagentic transport, free-electron density and mobility have been measured in the regime of filamentary current flow after the electric breakdown of *n*-GaAs at the temperature of liquid helium. The data show good agreement with those acquired by the geometrical magnetoresistance effect and by the optical Hall angle measurement. By comparing the mobilities obtained by independent techniques, arguments have been found indicating significant neutral impurity scattering in the post-breakdown regime. In the pre-breakdown regime variable range hopping has been concluded as the dominant transport mechanism.

INTRODUCTION

Although the occurrence of current controlled negative differential conductivity (SNDC) in *n*-GaAs and other moderately doped semiconductors at liquid-helium temperatures has been known for many years,[1,2] explanation of its mechanism is still a matter of controversy. While there is no doubt that the impact ionization of shallow impurities is the source of the order-of-magnitude increase in the conductivity, various processes have been proposed to explain the simultaneous decrease of the sustaining electric field, which leads to the observed current bistability. For example, some authors assume decreasing efficiency of the hot-electron capture,[3,4] while others take account of the increase of electron mobility due to the screening of ionized impurities[5] or due to the electron overheating effect.[2] Nevertheless, so far the greatest theoretical attention has been paid to the model of two-level generation-recombination kinetics[6,7] and to Monte-Carlo calculation based generalizations of this model.[8–10] This is primarily due to the fact that the latter approach has been proven to yield a solid theoretical basis for the explanation and modeling of the spontaneous formation of current carrying filaments,[11,12]which is characteristic in the post-breakdown regime of *n*-GaAs (Refs. 13–15) and SNDC materials generally.[16]

In spite of the almost quantitative agreement between numerical simulations and filament imaging experiments,[11,12] little experimental data are available on the transport parameters of the carriers in the filamentary regime. In this paper we report on measurements of electron mobility and density in the vicinity of the electric breakdown of *n*-GaAs. At first we will analyze the results of standard Hall measurement with regard to the inherent inhomogeneity of the current flow. The results corrected with respect to this inhomogeneity will be shown to agree with the data obtained from the geometrical magnetoresistance effect. Then, the optically and electrically detected magnetoresistance data will be combined to yield information about the electron-scattering mechanism. Finally, some conclusions will be drawn regarding the pre-breakdown conduction mechanism.

EXPERIMENT

Experimental setup

The measurments were performed on samples cut from two different layers grown by molecular beam epitaxy (MBE) on semi-insulating substrates. The first layer (PB) had an effective donor concentration $N_D^* = 2.6\times10^{15}\text{cm}^{-3}$ and electron mobility $\mu = 41\,000\ \text{cm}^{-2}/\text{V s}$ at 77 K, the second layer (PC) was less doped, $N_D^* = 1.9\times10^{15}\ \text{cm}^{-3}$, yielding a higher mobility of $\mu = 43\,000\ \text{cm}^{-2}/\text{V s}$ at 77 K but also a higher compensation ratio. Other parameters of the material are summarized in Table I(a). Two different sample geometries were prepared from each layer: bar-shaped samples with source and drain contacts on the short edges and four potential sensing dot contacts inside, and wide rectangular samples with two stripe contacts along the long

TABLE I. (a) Material parameters and (b) sample dimensions. The layer thicknesses in brackets correspond to the nondepleted parts of the epitaxial layers (Ref. 17). L_{SD} denotes the source–drain distance, w_s the sample width, d_l and d_H are the distances of the potential contacts in the longitudinal and transverse directions, respectively, and D_{pc} is their diameter.

(a)		
material	PB	PC
Layer thickness (μm)	4.3 (3.1)	4.3 (2.9)
N_D at 77 K (10^{15} cm^{-3})	3.1	2.5
N_A at 77 K (10^{15} cm^{-3})	0.5	0.6
μ at 77 K (10^3 cm^2/V s)	41	43
(b)		
Sample geometry	1	2
Designation	Hall	magnetoresistance
L_{SD} (mm)	3.65	1.05
w_s (mm)	1.5	4.2
d_l/d_H (mm)	2.7/0.9	
D_{pc} (mm)	0.15	

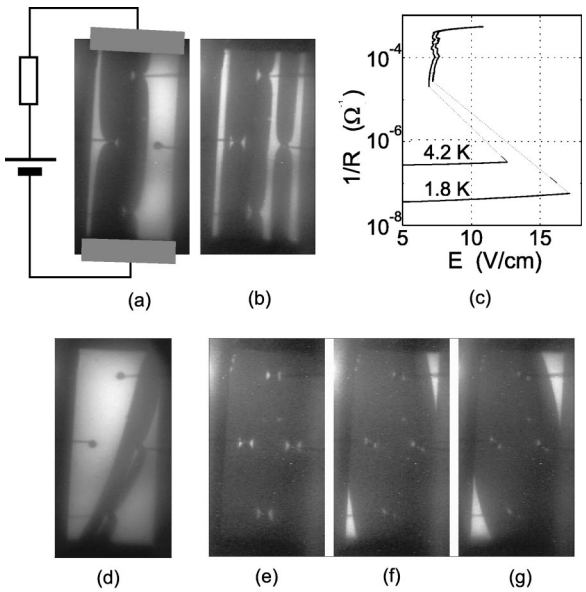

FIG. 1. (a), (b) Examples of filamentary current flow at $B_z=0$. (c) Conductance vs electric-field strength dependence for 1.8 and 4.2 K. (d) Example of filamentary current flow in a perpendicular magnetic field. (e) – (g) Filamentary current flow at sample filling current without (e) and with (f) and (g) magnetic field.

edges. The former geometry was used for standard Hall measurement (samples PB1, PC1), the latter for the magnetoresistance measurement (samples PB2, PC2). Dimensions of the samples are described in Table I(b).

Simultaneously with the electrical measurements, the spatial current distribution was imaged by the technique of photoluminescence quenching.[18] Typical examples of filamentary current images are seen in Figs. 1(a) and 1(b). The current is concentrated in sharp-bordered conducting channels, appearing as dark vertical stripes connecting the current contacts, which are schematically sketched at the bottom and the top of the image in Fig 1(a). Inside the current filaments obvious neckings are seen as the current passes the highly conducting areas of the floating dot contacts. An analogous filament-pinning effect may be observed also due to material imperfections.[19,20] The arrangement of filaments in Figs. 1(a) and 1(b) are obtained for the same current. This demonstrates that under identical external conditions many possible geometrical configurations of current carrying filaments can be found in the the post-breakdown regime. Correspondingly, multibranched current-voltage (I-V) characteristics are observed. In Fig. 1(c) only one such branch (for two different temperatures) is shown, which can be reproducibly obtained by increasing monotonously the bias voltage at some specific value of the bias resistor (here 20 kΩ); the characteristic is plotted in terms of the sample conductance and the driving longitudinal electric field. The vertical part of the characteristic reflects abrupt changes in the filament arrangement, as well as the continuous growth of filament widths.[19,20] The sample conductivity becomes almost constant as the whole width of the sample becomes filled with the high-conducting phase. Upon applying a perpendicular magnetic field the filaments are bent and tilted due to the Lorentz force,[15] as seen in Fig. 1(d). A significant deformation of the high-conducting area in a magnetic field occurs even in the case of high currents. Figures 1(e)–1(g) show three images at the same current well above the vertical part of the I-V characteristic. Growing bright parts of the low-conducting phase can be seen in the sample corners upon increasing the magnetic-field strength, Figs. 1(f) and 1(g).

Due to the inherent inhomogeneity of the conductance demonstrated above, it is obvious that the standard technique of obtaining the carrier mobility by measuring the Hall voltage is not applicable without further considerations. Primarily, the presence of multiple filaments must be excluded and, secondly, a conducting connection must be ensured between the current filament and the potential sensing electrodes. This latter requirement is difficult or even impossible to fulfill in the standard geometries like clover leaf or Hall bridge, where the potential contacts sit beside the current path.[21] Therefore, we decided to put two pairs of small dot contacts into the sample interior to measure the longitudinal and the transverse (Hall) electric fields.

Simulation-based interpretation of measurements

In designing the sample geometry, two requirements have been taken into account: contact spacing had to be much greater than their size in order to minimize local-field effects; on the other hand, the length-to-width ratio of the sample had still to be great enough to approach the ideal Hall-bar conditions. Both restrictions can be obeyed only to a certain practical degree. In order to interpret experimentally accessible data in terms of transport parameters, a numerical simulation of current flow in the real sample geometry has been performed. The model according to Refs. 15 and 22 has been used, based on the Drude formula for drift transport in crossed electric and magnetic fields:

$$\boldsymbol{j}=b_M e\mu n\begin{pmatrix}1 & -\tan(\Theta_H)\\ \tan(\Theta_H) & 1\end{pmatrix}\boldsymbol{\mathcal{E}}. \qquad (1)$$

Here $\boldsymbol{j}=(j_x,j_y)$ is the current density in the plane of the semiconductor film, $\boldsymbol{\mathcal{E}}=(\mathcal{E}_x,\mathcal{E}_y)$ is the electric field, Θ_H is the Hall angle, and $\tan(\Theta_H)=\mu_H B_z$. B_z is the normal magnetic field, e, n, and μ are, respectively, the electron charge, electron density, and mobility in the case of zero magnetic field, and $\mu_H=r_H\mu$ is the Hall mobility. The dimensionless coefficients b_M and r_H (Hall factor) depend on the carrier scattering mechanism and will be discussed later. This transport equation is used when numerically solving the continuity equation, $\boldsymbol{\nabla}\cdot\boldsymbol{j}=0$, along with the Dirichlet boundary conditions on the contact edges, and Neumann boundary conditions on the sample sides and the filament boundaries. Inside the potential contacts, enhanced conductivity (by a factor of 100) is assumed.

In Fig. 2(a) an example of the solution of the above problem is shown, assuming that the current flow is nonfilamentary, i.e., spread across the whole sample. This situation applies well to measurements in the pre-breakdown regime. Varying the magnetic-field strength (appearing only as the Hall angle Θ_H in the model), it is possible to acquire the corresponding values of voltages U_l and U_H accross the longitudinal and transverse pairs of potential contacts, respectively. Thus, a conversion function can be constructed as shown in Fig. 2(c), which replaces the simple linear dependence $\tan(\Theta_H)=U_H/U_l d_l/d_H$ valid in the case of the ideal

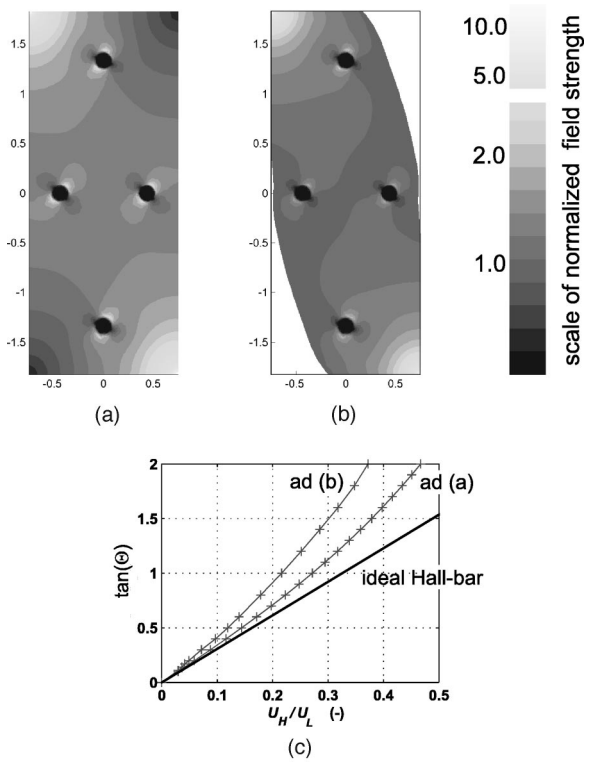

FIG. 2. Calculated distributions of field strength in the real sample geometry at Hall angle $\tan(\Theta_H)=1$. (a) Homogeneously conducting sample. (b) Sample with partially confined filament; note the constant field strength along the free filament boundary (its value is normalized to unity in the gray scale). (c) Hall angle Θ_H vs measurable voltage ratio for the ideal Hall-bar geometry (solid line), and for the nonfilamentary (lower-crossed line) and the filamentary (upper crossed line) current flow in the real sample geometry.

Hall-bar geometry (d_l/d_H is the geometry factor, see Table I). This function, in the form of a fitted polynomial, is used below to evaluate the mobility measurement in the pre-breakdown regime. Fitting coefficients for the sample dimensions used are shown in Table II.

In the post-breakdown regime, the filamentary current flow—unavoidable in a magnetic field—has to be taken into account by releasing the boundary of the conducting area from the boundary of the sample. The position of the free boundary is then sought in an iterative procedure, until an additional boundary condition of critical electric-field strength on the filament boundary is fulfilled.[15,22] An example of such a solution for $\Theta_H=\pi/4$ is shown in Fig. 2(b). Again, a conversion function $\tan(\Theta_H)=f(U_H/U_l)$ can be constructed, as shown in Fig. 2(c); coefficients of its polynomial representation are in Table II. Unlike the previous case

TABLE II. Polynomial coefficients of the conversion functions in the form $\tan(\Theta_H)=a_1U_H/U_l+a_3(U_H/U_l)^3$.

	a_1	a_3
Ideal Hall bar	3.07 ($=d_l/d_H$)	0
Homogeneous	3.34	4.41
Filament	4.18	8.59

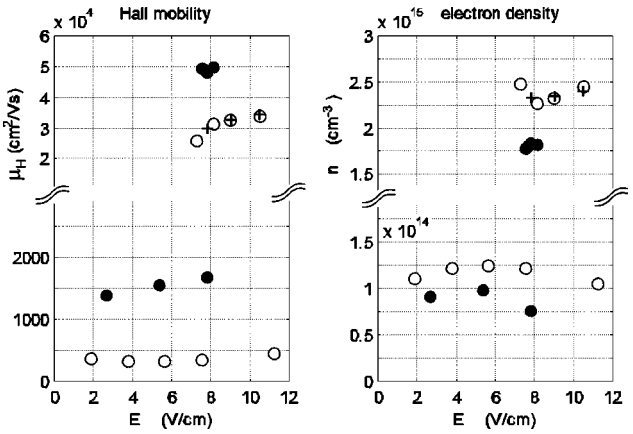

FIG. 3. Measured Hall mobilities and electron densities in the post-breakdown (upper parts) and pre-breakdown (lower parts) regimes. The data were corrected to allow for the real-sample geometry with the filamentary (post-brekdown regime) and the nonfilamentary (pre-breakdown regime) current flow. Solid circles belong to sample PC1, open circles and crosses to sample PB1. Crosses correspond to 1.8 K, all other points to 4.2 K.

of homogeneous conductivity, the solutions—and therefore the conversion function—are not freely scalable with the bias voltage. Therefore, they have been computed for the experimentally feasible situation in which the filament width is set equal to the sample width at $B_z=0$, and the corresponding current is then kept constant when varying the magnetic field.

RESULTS AND DISCUSSION

Hall-effect measurement

The Hall mobility and electron density acquired by the above procedure are plotted in Fig. 3. The most striking result is the order-of-magnitude difference in the measured mobility before and after the breakdown. At first sight, it seems that the Brooks-Herring formula for scattering on ionized impurities[23] is enough to explain this jump in mobility as it predicts a significant increase in the relaxation time with increasing free-electron density due to the more effective screening of the scattering potential. Moreover, the relaxation time of ionized impurity scattering rises with increasing electron energy.

There are, however, several reasons to asses the experimental results in pre-breakdown regime critically. First of all, it proved impossible to obtain reasonable pre-breakdown data at 1.8 K. Though the conductance was still in a well measurable range as seen from Fig. 1(c), the Hall voltage sank under the noise level even at magnetic fields of 1 T. Second, in a distinct range of magnetic fields, both samples exerted negative magnetoresistance with a minimum of about 0.5% below the magnetic-field free resistance at 4.2 K. Third, the temperature dependence of the pre-breakdown conductance is definitely not compliant with the activation law for the equilibrium free-electron density. Apparent activation energy was about 0.5 meV, being an order of magnitude less then the expected value for shallow donors. Based on the above arguments we suppose that the apparent Hall mobility determined at 4.2 K in the pre-breakdown regime of

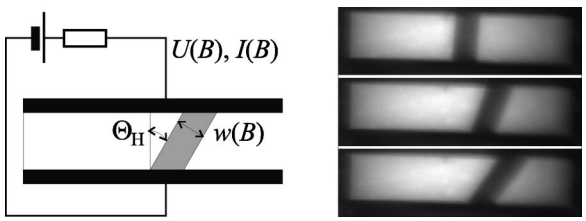

FIG. 4. Geometrical magnetoresistance effect in the filamentary regime of current flow. In the images on the right, the magnetic field rises from the top to the bottom as follows: $B_z = 29$, 103, and 211 mT.

both samples is due to the combination of the drift transport and variable range hopping. The latter mechanism is known to yield extremely low Hall-field values, negative magnetoresistance, as well as a specific temperature dependence.[24–26]

In the post-breakdown regime, the Hall mobilities of both samples increase to the same as or even above the values at 77 K. Moreover, there is no difference between values measured at the helium bath temperatures of 4.2 and 1.8 K. This agrees with the theoretical result of Gaa *et al.*[10] determining the electron temperature inside a current filament to be much higher than the lattice temperature. An obvious splitting of the transport parameters of the two samples in the filamentary regime should also be noticed, contrasting to their very similar values at 77 K.

Hall-angle and geometrical magnetoresistance measurement

In crossed electric and magnetic fields, the direction of the current flow is deflected from the electric-field direction by the Hall angle Θ_H according to Eq. (1). If not constrained by the sample edges, stripelike current filaments follow this angle, allowing us to measure the Hall angle directly by a protractor from the photoluminescence image,[27] Fig. 4. Such a measurement is independent of the sample current and filament width. Hall mobilities for samples PB2 and PC2, extracted from the measured Hall angles, are plotted in Fig. 5.

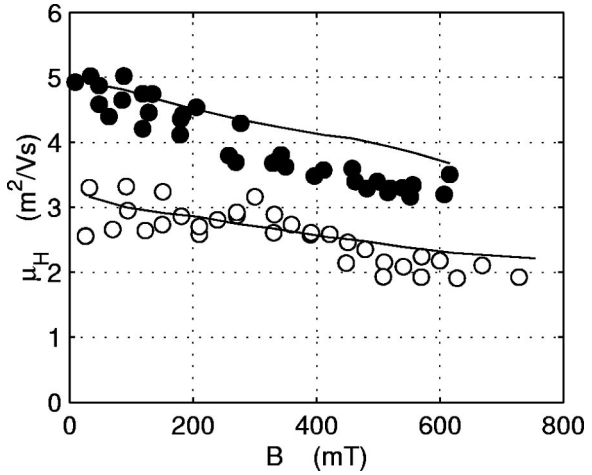

FIG. 5. Hall mobilities extracted optically from the Hall angle (single dots), and from the magnetoresistance (solid lines); the magnetoresistance data were evaluated by Eq. (2), assuming the denominator on the right-hand side was equal to one. Solid circles belong to sample PC2, open circles to sample PB2.

Very good agreement can be seen with Hall mobilites obtained by the standard Hall measurement according to Fig. 3.

Simultaneously with increasing Hall angle the resistance of a wide sample rises mainly due to a prolonged current path, which is referred to as geometrical magnetoresistance. Using Eq. (1) and assuming vanishing transverse electric field, the following equation can be obtained for the sample resistance R:

$$\frac{R(B_z)}{R_0}\,\frac{w(B_z)}{w_0}=\frac{[1+\tan(\Theta_H)^2]^{1/2}}{b_M[1+(r_H\omega_c\langle\tau\rangle)^2]}. \tag{2}$$

Here R_0 and w_0 denote sample resistance and filament width at $B_z=0$, respectively, ω_c is the cyclotron frequency, and $\langle\tau\rangle$ is the electron momentum relaxation time averaged over the electron energy distribution. The left-hand side of Eq. (2) can further be simplified to the sample voltage ratio $U(B_z)/U_0$, if a linear dependence of the filament width on the current is taken into account.[22,15] Factors b_M and r_H are also functions of τ:

$$b_M=\left\langle\frac{\tau}{1+(\omega_c\tau)^2}\right\rangle\langle\tau\rangle^{-1}, \tag{3a}$$

$$r_H=\left\langle\frac{\tau^2}{1+(\omega_c\tau)^2}\right\rangle\left\langle\frac{\tau}{1+(\omega_c\tau)^2}\right\rangle^{-1}\langle\tau\rangle^{-1}. \tag{3b}$$

From the quantities in Eq. (2), only the denominator on the right-hand side is not directly accesible by the experiment. Combining the optically measured Θ_H with the electrically measured sample voltage, experimental values of the expression in the denominator can be obtained. Suprisingly, within the few percent accuracy of the angle measurement this expression is identically equal to one in the whole range of the applied magnetic field. Assuming the low-field limit $(\omega_c\tau)^2\ll 1$, the denominator can indeed be shown to converge to one. However, as seen from Fig. 5, the product $\mu_H B_z$ clearly exceeds unity for the highest magnetic fields used, and the weak-field condition is thus not generally valid. Analogously to the Hall factor, two other conditions can be found, independently making the denominator expression converge to unity. Either the energy distribution function is δ-shaped, projecting out only one discrete value of τ by averaging over the energy, or the relaxation time τ is energy independent. The former possibility does not seem to apply. Though the electrons in filaments are hot, a moderate purity of the material as well as a relatively low electric field make the energy distribution rather broad. Also the Monte-Carlo simulations of the post-breakdown transport in *n*-GaAs reveal merely an increase in the high-energy tail of the distribution function.[28]

On the other hand, arguments can be found in favor of neutral impurity scattering, which is characterized by a dispersionless momentum relaxation time.[29,30] First, in doped GaAs at low temperature the rate of this process exceeds that of the lattice-scattering mechanisms,[23] and may become a mobility limiting process if ionized impurity scattering is weak.[3] Second, the concetration of neutral impurities $N_{NI}\approx N_D^0\approx N_D-N_A-n$ can be obtained using the data of Table I and the post-breakdown electron densities according to Fig. 3. The ratio of these concentrations in the layers PB and PC,

which is equal to the ratio of neutral impurity scattering rates, is approximately two. This value is close to the inverse ratio of the corresponding mobilities, which is approximately 1.7 according to Figs. 3 and 5. Applying Erginsoy's formula for the relaxation rate,[23] and estimating the mobility as $\mu = e\tau_{NI}/m^*$, absolute values of mobilities can be obtained of 4×10^4 and 8×10^4 $cm^2/V\,s$ for layers PB and PC, respectively. These lie in reasonable proximity of the experimental data, if the finite accuracy of the entering parameters and a further decrease of mobility due to the combined effect of other scattering processes is considered.

CONCLUSIONS

It has been shown that the galvanomagnetic transport in n-GaAs yields an experimental basis for transport parameter measurements even in the case of a filamentary current flow. The sample geometry with potential sensing contacts inside the sample and the simulation-based correction of the measured data have made it possible to use the standard Hall-effect technique. The results obtained by this method are shown to be in very good quantitative agreement with direct optical measurement of the Hall angle, based on the current filament tilting in a wide sample and its photoluminescence imaging. Magnetoresistance measurement in the same sample has proven to be a third method to confirm exactly the Hall-mobility data.

An independent knowledge of the Hall angle and the magnetoresistance data for the same sample offers a unique way to extract information about the scattering processes. Comparing the corresponding measurements we found arguments that indicate a significant role of neutral impurity scattering in the current filaments.

In the pre-breakdown regime, the Hall signal was found to collapse at temperature of 1.8 K. Supported by negative magnetoresistance and a specific temperature dependence of the conductivity we conclude that varibale range hopping is the dominant transport mechanism in this regime.

ACKNOWLEDGMENTS

The authors thank E. Schöll and H. Kostial for valuable discussions, S. Kreuzer for the sample structuring, and J. Hirschinger for his help during the first stage of the experiments. Support of the Humboldt Foundation is gratefully acknowledged by V.N. The work was also supported by Grant No. A1010011 of the GA CR and by the Deutsche Forschungsgemeinschaft.

[1] D.J. Oliver, Phys. Rev. **127**, 1045 (1962).
[2] I.B. Levinson, Fiz. Tverd. Tela **7**, 1362 (1965) [Sov. Phys. Solid State **7**, 1098 (1965)].
[3] V.C. Kieu, Phys. Status Solidi A **45**, 571 (1978).
[4] R.M. Westerwelt and S.W. Teitsworth, J. Appl. Phys. **57**, 5457 (1985).
[5] M. Kozhevnikov, B.M. Ashkinadze, E. Cohen, and A. Ron, Phys. Rev. B **52**, 4855 (1995).
[6] P.T. Landsberg and E. Schöll, J. Phys. C **9**, 1243 (1976).
[7] E. Schöll, *Nonequilibrium Phase Transitions in Semiconductors* (Springer-Verlag, New York, 1987).
[8] W. Quade, G. Hüpper, and E. Schöll, Phys. Rev. B **49**, 13 408 (1994).
[9] B. Kehrer, W. Quade, and E. Schöll, Phys. Rev. B **51**, 7725 (1995).
[10] M. Gaa, R.E. Kunz, and E. Schöll, Phys. Rev. B **53**, 15 971 (1996).
[11] M. Gaa, R.E. Kunz, E. Schöll, W. Eberle, J. Hirschinger, and W. Prettl, Semicond. Sci. Technol. **11**, 1646 (1996).
[12] G. Schwarz, C. Lehmann, A. Reimann, E. Schöll, J. Hirschinger, W. Prettl, and V. Novák, Semicond. Sci. Technol. **15**, 593 (2000).
[13] K.M. Mayer, J. Parisi, and R.P. Huebener, Z. Phys. B: Condens. Matter **71**, 171 (1988).
[14] K. Aoki, U. Rau, J. Peinke, J. Parisi, and R.P. Huebener, J. Phys. Soc. Jpn. **59**, 420 (1990).
[15] J. Hirschinger, F.-J. Niedernostheide, W. Prettl, and V. Novák, Phys. Rev. B **61**, 1952 (2000).
[16] K.M. Ridley, Proc. Phys. Soc. London **82**, 954 (1963).
[17] E.H.C. Parker, *The Technology and Physics of Molecular Beam Epitaxy* (Plenum, New York, 1985).
[18] W. Eberle, J. Hirschinger, U. Margull, W. Prettl, V. Novák, and H. Kostial, Appl. Phys. Lett. **68**, 3329 (1996).
[19] S.A. Proshin, V.G. Golubev, S. Würfl, J. Spangler, A. Schilz, and W. Prettl, Semicond. Sci. Technol. **8**, 1298 (1993).
[20] H. Klimenta, M. Alshuth, W. Prettl, and H. Kostial, Phys. Status Solidi A **176**, 1017 (1999).
[21] M.G. Lukashevich, M. Bogershausen, and H. Micklitz, Phys. Status Solidi A **44**, 377 (1994).
[22] V. Novák, J. Hischinger, W. Prettl, and F.-J. Niedernostheide, Semicond. Sci. Technol. **13**, 756 (1998).
[23] C.M. Wolfe, G.E. Stillman, and W.T. Lindley, J. Appl. Phys. **41**, 3088 (1970).
[24] R. Mansfield, in *Hopping Transport in Solids*, edited by M. Pollak and B. Shklovskii (Elsevier, New York, 1991).
[25] M. Benzaquen, D. Walsh, and K. Mazuruk, Phys. Rev. B **36**, 4748 (1987).
[26] M. Benzaquen, D. Walsh, and K. Mazuruk, Phys. Rev. B **38**, 10 933 (1988).
[27] V. Novák, J. Hirschinger, F.-J. Niedernostheide, W. Prettl, M. Cukr, and J. Oswald, Phys. Rev. B **58**, 13 099 (1998).
[28] H. Kostial, M. Asche, R. Hey, K. Ploog, B. Kehrer, W. Quade, and E. Schöll, Semicond. Sci. Technol. **10**, 775 (1995).
[29] C. Erginsoy, Phys. Rev. **79**, 1013 (1950).
[30] N. Sclar, Phys. Rev. **104**, 1559 (1956).